A highly selective fluorescent probe for cadmium ions in aqueous solution and living cells

ARTICLE *in* CHEMICAL COMMUNICATIONS · JANUARY 2014

Impact Factor: 6.83 · DOI: 10.1039/c3cc48668k · Source: PubMed

8 AUTHORS, INCLUDING:

Yuan Caixia
Shanxi University
19 PUBLICATIONS **284** CITATIONS
SEE PROFILE

Chuan Dong
Shanxi University
201 PUBLICATIONS **2,030** CITATIONS
SEE PROFILE

Qin Hu
Hong Kong Baptist University
16 PUBLICATIONS **71** CITATIONS
SEE PROFILE

ChemComm

COMMUNICATION

View Article Online
View Journal | View Issue

A highly selective fluorescent probe for cadmium ions in aqueous solution and living cells†

Cite this: *Chem. Commun.*, 2014, **50**, 2498

Received 13th November 2013,
Accepted 10th January 2014

DOI: 10.1039/c3cc48668k

www.rsc.org/chemcomm

Qiaoling Liu,[ab] Lixia Feng,[ab] Caixia Yuan,[a] Lin Zhang,[a] Shaomin Shuang,[a] Chuan Dong,*[a] Qin Hu[c] and Martin M. F. Choi*[c]

An organic salt based on double 1,3,4-oxadiazole derivatives as fluorophores and BAPTA as a receptor has been designed for detection of Cd^{2+}. The fluorescent probe exhibits high selectivity for Cd^{2+} and a low detection limit of 20 nM in aqueous solution, making it useful for Cd^{2+} imaging in living MCF-7 cells.

Cadmium (Cd), one of the very important metallic elements, is extensively used in many areas such as metallurgy, electroplating, the war industry, nickel–cadmium batteries, pigments, and semiconducting quantum dots and rods.[1] The extensive use of Cd leads to serious environmental and health problems including lung, prostatic, and renal cancers.[2] The carcinogenic effect of Cd exposure on laboratory rats showed that between 0.0 and 2.5 μM of $CdCl_2$ could induce tumour incidence and multiplicity; a dose of 2.5 μM could significantly elevate the prostatic tumour incidence; and a 20 or 40 μM dosage would strongly induce Leydig cell tumour incidence.[3a] Moreover, Cd can accumulate in the human body and cause renal dysfunction, calcium metabolism disorders and other relevant forms of diseases. The Itai-Itai disease in Japan in the 1940s is a typical example.[3] Thus, there is a great demand for developing a facile method with high sensitivity and good selectivity to monitor Cd in the environment and in biological samples.

Fluorescent probes based on metal ion induced changes in fluorescence appear to be particularly advantageous owing to their simple operation and low detection limit. Cadmium ion (Cd^{2+}) probes with different detection mechanisms such as photoinduced electron transfer,[4] intramolecular charge transfer (ICT),[5] chelation-enhanced fluorescence,[6] metal–ligand charge transfer,[7] excimer/exciplex formation,[8] intermolecular hydrogen bonding,[9] and fluorescence resonance energy transfer[10] have been developed. Unfortunately, most of them suffer from UV excitation,[5,8,11] poor water-solubility[11,12] or poor selectivity between Cd^{2+} and Zn^{2+}.[13] Recently several water-soluble Cd^{2+} probes have been introduced but their performances are still far from satisfactory. For instance, there is a relatively small Stokes shift (20 nm) for the Cd^{2+} sensor,[4] or the detection limit is higher than the level of the maximum limit in water stipulated by the US EPA and WHO (4–40 nM).[14] As such, it is highly desirable to develop a new Cd^{2+} probe with a better performance in sensitivity and selectivity in an aqueous environment.

To our knowledge, fluorescent ICT-based probes have been widely exploited for the detection of cations owing to their strong emission intensity and large Stokes shift. These attributes arise from the π-electron conjugation system between the electron donor and the electron acceptor, facilitating the ICT process. Once the ICT-based probe has coordinated with metal ions, the ICT is inhibited or reduced with concomitant changes in not only the energy gap between the lowest unoccupied molecular orbital (LUMO) and the highest occupied molecular orbital (HOMO) but also the absorption and fluorescence intensity and spectral shifts.[15] To date, there are only a few Cd^{2+} probes incorporating the ICT concept. Herein we first report a highly selective and sensitive probe for Cd^{2+} detection based on a novel bichromophoric and bifluorophoric molecule (OBO) and the ICT processes.

The Cd^{2+} probe (OBO) was designed by incorporating a multifunctional ionophore 1,2-bis(2-aminophenoxy)ethane-*N*,*N*,*N*′,*N*′-tetraacetic acid (BAPTA) as the Cd^{2+} receptor with two 1,3,4-oxadiazole derivatives (OXD) to form a sandwich compound OXD–BAPTA–OXD possessing an ICT capability. First, OXD was chosen as the bichromophore and bifluorophore owing to its large Stokes shift and high fluorescence quantum yield. Second, BAPTA is well known for its high selectivity to various metal ions. Third, OBO is a water-soluble salt which can completely dissolve in water to selectively bind with Cd^{2+} in aqueous and cellular environments. Another major attribute of OBO is that it does not respond to most divalent metal ions under visible light excitation.

[a] *Institute of Environmental Science, and School of Chemistry and Chemical Engineering, Shanxi University, Taiyuan 030006, P. R. China. E-mail: dc@sxu.edu.cn; Fax: +86-351-7018613; Tel: +86-351-7018613*
[b] *Department of Chemistry, Taiyuan Normal University, Taiyuan 030031, P. R. China*
[c] *Department of Chemistry, Hong Kong Baptist University, 224 Waterloo Road, Kowloon Tong, Hong Kong SAR, P. R. China. E-mail: mfchoi@hkbu.edu.hk; Fax: +86-852-34117348; Tel: +86-852-34117839*

† Electronic supplementary information (ESI) available: Detailed synthetic procedures, supplementary figures, NMR spectra and the mass spectrum. See DOI: 10.1039/c3cc48668k

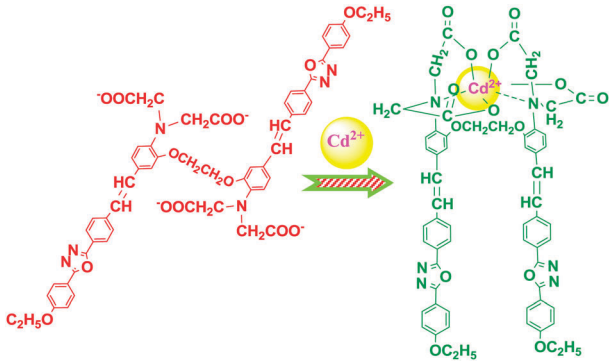

Scheme 1 Reaction mechanism of OBO with Cd^{2+}.

The detailed synthetic routes and confirmation of the chemical structures of the OBO-ester (the OBO precursor) and OBO by ^{1}H and ^{13}C nuclear magnetic resonance spectroscopy, mass spectrometry, and elemental analysis are provided in the ESI† (Fig. S1–S5). Scheme 1 illustrates the chemical structure and reaction mechanism of OBO with Cd^{2+}.

The photophysical properties of OBO are assessed under physiological conditions (50 mM HEPES, 0.10 M KCl, pH 7.2). Fig. 1 depicts the absorption spectra of OBO in the presence of various concentrations of Cd^{2+}. Free OBO exhibits two absorption bands at 304 nm ($\varepsilon = 3.82 \times 10^4\ M^{-1}\ cm^{-1}$) and 380 nm ($\varepsilon = 5.82 \times 10^4\ M^{-1}\ cm^{-1}$), corresponding to the π–π* transition and ICT bands, respectively. Upon addition of Cd^{2+}, the π–π* transition band decreases whereas the ICT band exhibits a hypsochromic shift to a new band at 354 nm ($\varepsilon = 7.18 \times 10^4\ M^{-1}\ cm^{-1}$), accompanied by two isosbestic points at 313 and 370 nm. The ratio of absorbance at 354 nm to that at 405 nm (A_{354}/A_{405}) increases with the addition of Cd^{2+} concentrations (Fig. S6 in the ESI†), indicating the formation of complex between OBO and Cd^{2+}. Similar results were obtained by taking the ratio of absorbance at 354 nm to that at 380 nm. The formation of the OBO–Cd^{2+} complex is further confirmed by ^{1}H NMR spectra and the quantum chemical calculations. Herein, the choice of 405 nm is in line with the use of laser-induced excitation to capture the living cell image incorporated with the OBO-ester and Cd^{2+} under the confocal fluorescence microscope (*vide infra*).

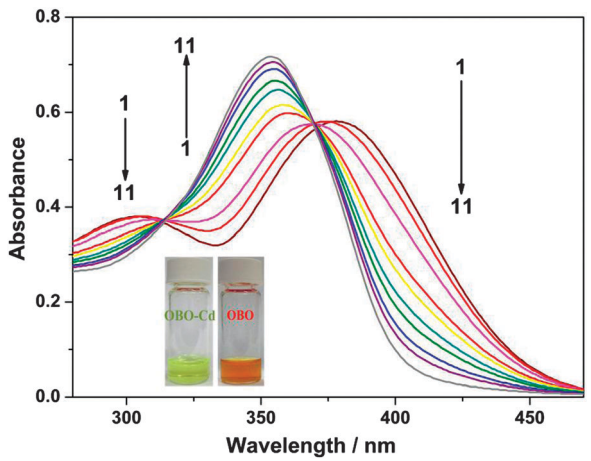

Fig. 1 Absorption spectra of 10.0 μM OBO in 50 mM HEPES (pH 7.2) containing 0.10 M KCl at various concentrations (1–11: 0.0, 1.0, 2.0, 3.0, 4.0, 5.0, 6.0, 7.0, 8.0, 9.0, and 10.0 μM) of Cd^{2+} ion. The bottom inset displays images of OBO with (left) and without (right) Cd^{2+}.

The ^{1}H NMR spectrum of OBO–Cd^{2+} shows that the protons (H_a and H_b) in *N*-methylene of acetate and the 3-position of benzene display the upfield shifts when OBO binds to Cd^{2+} (Fig. S7 in the ESI†), suggesting that the binding site is BAPTA. The quantum chemical calculation also supports this conclusion. Fig. S8 (ESI†) depicts the optimal geometries of free OBO and the OBO–Cd^{2+} complex, which indicate the structure and the binding site at the BAPTA moiety of OBO. It clearly visualizes that the Cd^{2+} ion binds to the oxygen and nitrogen atoms of BAPTA. The main coordinated bond lengths at this binding site are summarised in Table S1 (ESI†). The main coordinated bond lengths of Cd–O1, Cd–O2, Cd–O3, and Cd–O4 are slightly shorter than the reported Cd–O bond length, suggesting a strong interaction between the tetra-carboxyl groups and Cd^{2+}. By contrast, the Cd–O5 and Cd–O6 bond lengths are longer and exceed the range of the bond force, inferring that the phenoxyethane moieties have almost no interaction with Cd^{2+}. The Cd–N7 and Cd–N8 bond lengths are longer than the usual Cd–N bond length, inferring a weaker interaction between the N atoms and Cd^{2+}.[16] Tables S2 and S3 (ESI†) display the ground-state energies and Cartesian coordinates of OBO and the OBO–Cd^{2+} complex in water at the B3LYP/LanL2DZ+6-31G* level. These results again corroborate the formation of OBO–Cd^{2+} complex with the binding site at BAPTA.

Fig. 2 depicts the emission spectra of OBO upon the addition of various concentrations of Cd^{2+} at an excitation wavelength of 405 nm. Free OBO exhibits an emission maximum (λ^{fl}_{max}) of 594 nm with an enormous Stokes shift of 189 nm. The quantum yield (φ) is 0.024. Upon addition of Cd^{2+}, the λ^{fl}_{max} undergoes a hypsochromic shift to 532 nm with an increase in fluorescence and φ is 0.078. The inset displays the changes in emission intensities at 532 and 594 nm, respectively by plotting ($F - F_o$) against the concentration of Cd^{2+}, where F and F_o are the emission intensities with and without Cd^{2+}, respectively. It is clearly seen that the emission intensities at 532 and 594 nm increase with the increase in the concentration of Cd^{2+}. A good linear relationship is observed between ($F - F_o$) and [Cd^{2+}] (0.0–0.40 μM). The detection limit is found to be 20 nM (3σ/slope), demonstrating that OBO is a highly sensitive probe for Cd^{2+}.

To gain further insight into the spectral properties, the quantum chemical calculations are conducted by the Gaussian 09 program. The geometric parameters of OBO and OBO–Cd^{2+} are optimised by the hybrid Becke three-parameter Lee–Yang–Parr exchange correlation functional (B3LYP) method[17] with LanL2DZ+6-31G* mixed basis set (LanL2DZ[18] for Cd and 6-31G* for other atoms). Fig. S9 (ESI†) shows that the electrons of free OBO are localised on one side in the HOMO and the ethoxyphenyl group does not participate in the rearrangement of electrons. A total electron transfer from one side to another is observed between the HOMO and the LUMO. When OBO binds with Cd^{2+}, the BAPTA-Cd moiety is formed which functions as a bridge to connect the two OXO fluorophores. Electrons are localised on the whole molecule of the HOMO, making the π-conjugated system larger and preserving the ICT process. However, the calculated energy gap between the LUMO and the HOMO of OBO–Cd^{2+} (3.171 eV) is larger than that of free OBO (2.567 eV). This is in agreement with the hypsochromic shift of the absorption and

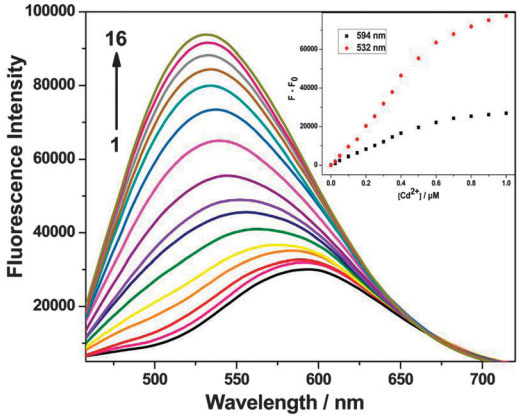

Fig. 2 Fluorescence emission spectra of 1.0 μM OBO in 50 mM HEPES (pH 7.2) containing 0.10 M KCl at various concentrations (1–16: 0.0, 0.025, 0.05, 0.1, 0.15, 0.2, 0.25, 0.3, 0.35, 0.4, 0.5, 0.6, 0.7, 0.8, 0.9, and 1.0 μM) of Cd^{2+} at an excitation wavelength of 405 nm. The inset displays ($F - F_o$) against concentration of Cd^{2+}, where F and F_o are the fluorescent intensities at 532 and 594 nm with and without Cd^{2+}, respectively.

emission spectra of OBO upon the formation of an OBO–Cd^{2+} complex. In summary, the π-conjugated system could enhance the fluorescence intensity and the ICT spectrum of OBO is hypsochromically shifted upon complexation with Cd^{2+}.

The stoichiometric ratio of OBO–Cd^{2+} complex is determined as 1 : 1 using Job's method (Fig. S10 in the ESI†). Hill's plot is applied to determine the dissociation constant of the OBO–Cd^{2+} complex to be 116.0 ± 27.0 nM (Fig. S11 in the ESI†), suggesting that the affinity of OBO to Cd^{2+} is much larger than other reported Cd^{2+} probes.[4,5b,6,12b] The fluorescence lifetimes of the free OBO and OBO–Cd^{2+} complex determined from time-resolved fluorescence spectroscopy are 1.41 and 1.48 ns at an excitation wavelength of 405 nm, respectively.

The fluorescence titration of OBO with various metal ions is depicted in Fig. S12a (ESI†). Among these metal ions, OBO displays excellent selectivity to Cd^{2+} with a strong fluorescence enhancement while other bivalent metal ions exhibit slight fluorescence quenching on OBO. Most importantly, OBO has almost no response to Zn^{2+} and is thus superior to other Cd^{2+} probes which often suffer from Zn^{2+} interference.[13] In addition, the co-existence of other bivalent metal ions do not affect the measurement of Cd^{2+} (Fig. S12b in the ESI†), demonstrating that OBO possesses excellent selectivity to Cd^{2+} over other bivalent metal ions. Fluorescent pH titration in the biologically relevant pH range (5.5–9.0) shows that the optimal working pH of OBO or the OBO–Cd^{2+} complex is 7.0 (Fig. S13 in the ESI†) which should meet their uses under a physiological environment.

In order to examine the ability of OBO to track the intracellular Cd^{2+} level, OBO-ester was employed for the cell permeability. MCF-7 cells were incubated with OBO-ester (5.0 μM) for 30 min at 37 °C, and then the ester was converted to the active form of OBO inside the cells by intracellular esterase, allowing the intracellular Cd^{2+} to be deciphered in the cytosol. Then exogenous Cd^{2+} was further introduced *via* incubation with 5.0 μM $CdCl_2$ for another 30 min. The images were recorded at 570–610 and 510–550 nm under the excitation wavelength of 405 nm (Fig. 3b and c). Fig. 3a depicts the bright field transmission image of the cells under a confocal microscope. A very clear cell image is observed. The cells turn to red

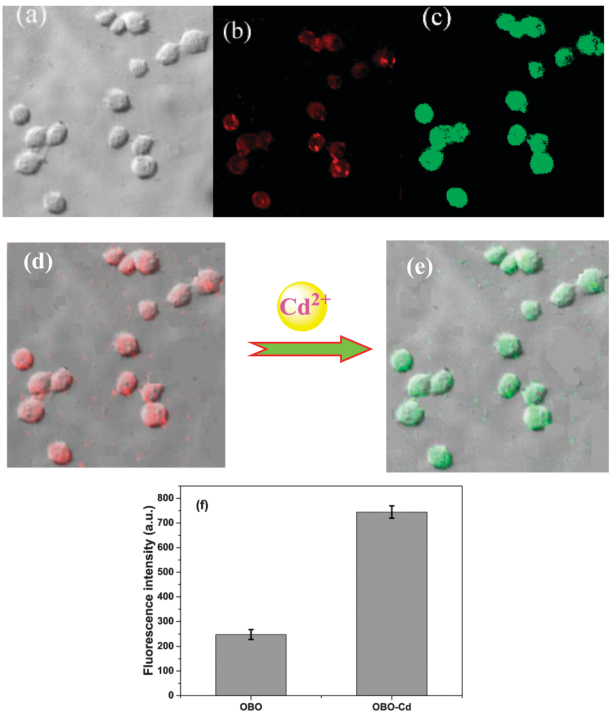

Fig. 3 Confocal fluorescent images of MCF-7 cells stained with 5.0 μM OBO-ester at an excitation wavelength of 405 nm: (a) bright field transmission image of MCF-7 cells incubated with OBO-ester. (b) Fluorescence image of MCF-7 cells incubated with OBO-ester at emission 570–610 nm. (c) Fluorescence image of MCF-7 cells incubated with OBO-ester for 30 min and then further incubated with 5.0 μM $CdCl_2$ for 30 min at emission 510–550 nm. (d) Images (a) and (b) are overlapped. (e) Images (a) and (c) are overlapped. (f) Comparison of the average intracellular fluorescence intensity with OBO at 570–610 nm and OBO–Cd^{2+} at 510–550 nm. Data are expressed as mean ± standard derivation of 10 cells.

after they have been exposed to OBO-ester, suggesting the penetration of OBO-ester into the cell. The cells are changed to bright green after they have been incorporated with Cd^{2+}, demonstrating that Cd^{2+} can permeate into the cells and bind with OBO to form OBO–Cd^{2+}. Fig. 3d and e presents the fluorescence images of the MCF-7 incorporated with OBO-ester in the absence and presence of Cd^{2+}, respectively. It is clear that OBO can stain the cells and also indicate the presence of Cd^{2+}. Moreover, Fig. 3f shows the mean fluorescent intensities of each cell captured at 570–610 and 510–550 nm, respectively. The emission intensity at 510–550 nm is about three times larger than that at 570–610 nm, corroborating that the emission intensity of OBO is enhanced in the presence of Cd^{2+} as shown in Fig. 2. Our results demonstrate that OBO can be potentially useful for imaging Cd^{2+} in living cells under a confocal laser scanning microscope.

In summary, we have successfully designed an organic salt as a fluorescent probe for Cd^{2+} based on the ICT principle. This probe exhibits a large Stokes shift of 189 nm and a low detection limit of 20 nM Cd^{2+} under visible excitation. Moreover, its high sensitivity and selectivity to Cd^{2+} in an aqueous environment facilitate the possible application of OBO in imaging Cd^{2+} in living cells, further demonstrating its potential for Cd^{2+} detection in biological systems.

This work is supported by the Hundred Talent Programme of Shanxi Province, and the National Natural Science Foundation of China (21175086 and 21175087).

Notes and references

1 (*a*) A. M. S. Mendes, G. P. Duda, C. W. A. do Nascimento and M. O. Silva, *Sci. Agric.*, 2006, **63**, 328–332; (*b*) L. Järup and A. Akesson, *Toxicol. Appl. Pharmacol.*, 2009, **238**, 201–208.
2 (*a*) C. C. Bridges and R. K. Zalups, *Toxicol. Appl. Pharmacol.*, 2005, **204**, 274–308; (*b*) B. J. Julin, A. Wolk, L. Bergkvist, M. Bottai and A. Akesson, *Cancer Res.*, 2012, **72**, 1459–1466.
3 (*a*) M. P. Waalkes, S. Rehm and C. W. Riggs, *Cancer Res.*, 1988, **48**, 4656–4663; (*b*) M. P. Waalkes, *Mutat. Res.*, 2003, **533**, 107–120.
4 T. Cheng, Y. Xu, S. Zhang, W. Zhu, X. Qian and L. Duan, *J. Am. Chem. Soc.*, 2008, **130**, 16160–16161.
5 (*a*) Z. Liu, C. Zhang, W. He, Z. Yang, X. Gao and Z. Guo, *Chem. Commun.*, 2010, **46**, 6138–6140; (*b*) Y. Tan, J. Gao, J. Yu, Z. Wang, Y. Cui, Y. Yang and G. Qian, *Dalton Trans.*, 2013, **42**, 11465–11470.
6 Z. Li, P. Xi, L. Huang, G. Xie, Y. Shi, H. Liu, M. Xu, F. Chen and Z. Zeng, *Inorg. Chem. Commun.*, 2011, **14**, 1241–1244.
7 W.-L. Gong, M. P. Aldred, G.-F. Zhang, C. Li and M.-Q. Zhu, *J. Mater. Chem. C*, 2013, **1**, 7519–7525.
8 A. Sahana, A. Banerjee, S. Lohar, S. Guha, S. Das, S. K. Mukhopadhyay and D. Das, *Analyst*, 2012, **137**, 3910–3913.
9 H. H. Lee, S. H. Jung, S. Park, K. M. Park and J. H. Jung, *New J. Chem.*, 2013, **37**, 2330–2335.
10 Y. Li, L. Li, X. Pu, G. Ma, E. Wang, J. Kong, Z. Liu and Y. Liu, *Bioorg. Med. Chem. Lett.*, 2012, **22**, 4014–4017.
11 (*a*) X. L. Tang, X. H. Peng, W. Dou, J. Mao, J. R. Zheng, W. W. Qin, W. S. Liu, J. Chang and X. J. Yao, *Org. Lett.*, 2008, **10**, 3653–3656; (*b*) G. M. Cockrell, G. Zhang, D. G. Van Derveer, R. P. Thummel and R. D. Hancock, *J. Am. Chem. Soc.*, 2008, **130**, 1420–1430.
12 (*a*) T. Cheng, T. Wang, W. Zhu, Y. Yang, B. Zeng, Y. Xu and X. Qian, *Chem. Commun.*, 2011, **47**, 3915–3917; (*b*) L. Xin, Y. Z. Chen, L. Y. Niu, L. Z. Wu, C. H. Tung, Q. X. Tong and Q. Z. Yang, *Org. Biomol. Chem.*, 2013, **11**, 3014–3019.
13 (*a*) X. Jiang, B. G. Park, J. A. Riddle, B. J. Zhang, M. Pink and D. Lee, *Chem. Commun.*, 2008, 6028–6030; (*b*) K. M. K. Swamy, M. J. Kim, H. R. Jeon, J. Y. Jung and J. Yoon, *Bull. Korean Chem. Soc.*, 2010, **31**, 3611–3616.
14 G. C. Midya, S. Paladhi, S. Bhowmik, S. Saha and J. Dash, *Org. Biomol. Chem.*, 2013, **11**, 3057–3063.
15 X. Li, X. Gao, W. Shi and H. Ma, *Chem. Rev.*, 2014, **114**, 590–659.
16 (*a*) B. J. Carra, S. M. Berry, R. D. Pike and D. C. Bebout, *Dalton Trans.*, 2013, **42**, 14424–14431; (*b*) W. Yuan, T. Liu, Z. Guo, H. Li and R. Cao, *J. Mol. Struct.*, 2010, **965**, 82–88.
17 A. D. Becke, *J. Chem. Phys.*, 1993, **98**, 5648–5653.
18 P. J. Hay and W. R. Wadt, *J. Chem. Phys.*, 1985, **82**, 270–283.